Contents lists available at ScienceDirect

EBioMedicine

journal homepage: www.elsevier.com/locate/ebiom

Research paper

Metabolomic analysis of a selective ABCA1 inducer in obesogenic challenge provides a rationale for therapeutic development

Cutler T. Lewandowski[a], Md.Wasim Khan[b], Manel BenAissa[a], Oleksii Dubrovskyi[a], Martha Ackerman-Berrier[c], Mary Jo LaDu[d], Brian T. Layden[b,*,1], Gregory R.J. Thatcher[c,*,1]

[a] Department of Pharmaceutical Sciences, University of Illinois at Chicago, Chicago, IL, USA
[b] Department of Medicine, University of Illinois at Chicago, 835 S. Wolcott St., Chicago, IL 60612, USA
[c] Department of Pharmacology and Toxicology, University of Arizona, 1295N. Martin, Tucson, AZ 85721, USA
[d] Department of Anatomy and Cell Biology, University of Illinois at Chicago, Chicago, IL, USA

A B S T R A C T

Background: Therapeutic agents with novel mechanisms of action are needed to combat the growing epidemic of type 2 diabetes (T2D) and related metabolic syndromes. Liver X receptor (LXR) agonists possess preclinical efficacy yet produce side effects due to excessive lipogenesis. Anticipating that many beneficial and detrimental effects of LXR agonists are mediated by ABCA1 and SREPB1c expression, respectively, we hypothesized that a phenotypic optimization strategy prioritizing selective ABCA1 induction would identify an efficacious lead compound with an improved side effect profile over existing LXRβ agonists.
Methods: We synthesized and characterized a novel small molecule for selective induction of ABCA1 vs. SREBP1c in vitro. This compound was evaluated in both wild-type mice and a high-fat diet (HFD) mouse model of obesity-driven diabetes through functional, biochemical, and metabolomic analysis.
Findings: Six weeks of oral administration of our lead compound attenuated weight gain, glucose intolerance, insulin signaling deficits, and adiposity. Global metabolomics revealed suppression of gluconeogenesis, free fatty acids, and pro-inflammatory metabolites. Target identification linked these beneficial effects to selective LXRβ agonism and PPAR/RXR antagonism.
Interpretation: Our observations in the HFD model, combined with the absence of lipogenesis and neutropenia in WT mice, support this novel approach to therapeutic development for T2D and related conditions.

1. Introduction

Nuclear receptors are therapeutic targets for type 2 diabetes (T2D) and related metabolic conditions. PPARγ agonists (e.g. pioglitazone) are approved for clinical use but have fallen out of favor due to side effects related to cardiovascular (CV) risk and emergence of drugs with CV benefit. The liver X receptor (LXR) represents a nuclear receptor target that has yet to be translated to the clinic. LXR agonists, e.g. T0901317 and GW3965, correct glucose homeostasis and insulin signaling in rodents [1-7]; however, SREBP1c induction via LXR agonism causes hypertriglyceridemia and steatohepatitis [8].

A key mechanism regulating beneficial effects of LXR nuclear receptor agonists is increased expression of cholesterol transporter ABCA1. Patients with T2D exhibit decreased ABCA1 expression [9], while tissue-specific Abca1 knockout in rodents impairs insulin signaling [10]. ABCA1 expression inversely correlates with retinal degeneration [11], diabetic kidney injury [12], atherosclerotic plaque development [13], and Alzheimer's disease-related pathology and cognitive deficits [14,15]. ABCA1 deficiency in macrophages causes proinflammatory gene expression and cytokine release [16], and human loss-of-function Abca1 mutations are associated with systemic inflammation [17,18]. ABCA1 can mediate the anti-inflammatory effects of LXR [19]. Moreover, LXR agonists can directly modulate gene expression related to glucose homeostasis and inflammation [20,21], while also decreasing weight gain and providing vascular and cardiac protection [4,22].

We pursued a novel phenotypic approach to identify small molecules that induce cellular ABCA1 expression, in contrast to a strategy that optimizes molecules for binding affinity and agonist potency at LXR isoforms. Specifically, we screened for non-lipogenic ABCA1 inducers that increase ABCA1 expression, but not that of SREBP1c, a transcription factor that promotes hepatic triglyceride (TG) synthesis [23]. While biased toward LXR agonists because the Abca1 promoter

Research in Context

Evidence before the study

Increasing activity or expression of the cholesterol transport protein ABCA1 has been proposed as a therapeutic target for type 2 diabetes and related conditions such as cardiovascular disease and Alzheimer's disease. Expression of ABCA1 is controlled by nuclear receptor transcription factors, particularly liver X receptor (LXR). Numerous LXRβ agonists have been developed to mediate several beneficial effects such as reverse cholesterol transport, anti-inflammatory activity, and enhanced insulin sensitivity. To date, however, pursuit of LXRβ has failed as a therapeutic approach because of lipogenesis, hypertriglyceridemia, liver steatosis, and neutropenia, often mediated by LXRα.

Added value of the study

This study describes a newly synthesized non-lipogenic ABCA1 inducer, termed CL2-57, that enhanced ABCA1 expression, increased sensitivity of liver and muscle tissue to insulin, and reduced inflammatory signaling in a high-fat diet (HFD) mouse model. Moreover, the unique combination of LXRβ partial agonist and PPAR/RXR antagonist activity prevented development of hypertriglyceridemia and neutropenia; and, notably, fatty acids and triglycerides were significantly reduced in HFD mice following compound treatment.

Implications of all the available evidence

Despite challenges in translating LXRβ agonists to the clinic, multiple studies have shown therapeutic potential in type 2 diabetes and related metabolic syndromes. A phenotypic drug discovery strategy overcame the limitations of focusing entirely on LXRβ engagement, identifying a non-lipogenic ABCA1 inducer that elicited multiple beneficial therapeutic actions while avoiding adverse effects that have blocked development of LXRβ agonists as drugs. Further optimization and development of non-lipogenic ABCA1 inducers can utilize this novel approach leading to an effective and safe drug candidate.

sequence contains an LXR response element, we hypothesized that a small molecule that induces ABCA1, with small or negligible SREBP1c effects, would yield beneficial effects on reverse cholesterol transport (RCT) and glucose metabolism, without adverse lipogenic activity, regardless of the specific receptor target through which it acted.

The non-lipogenic ABCA1 inducer synthesized and profiled in this study, CL2-57, was tested in the high-fat diet (HFD) mouse model of obesity-driven T2D. Herein, we demonstrate a robust and unique phenotype: improved glucose tolerance and insulin sensitivity; reduced weight gain and adiposity accompanied by significant TG reductions; and attenuated inflammation. For comprehensive analysis, we also employed global metabolomics profiling, which highlighted gluconeogenesis and fatty acid metabolism as key pathways modulated by CL2-57 in HFD mice. Target deconvolution highlighted the actions of CL2-57 as an LXRβ agonist and weak PPAR/RXR antagonist. Recent medicinal chemistry efforts, focused on optimizing potency and selectivity towards LXRβ, have stalled in early clinical trials: for example, BMS-852927, completed Phase I trials but caused significant neutropenia [24]. Our results demonstrate the ability of phenotypic drug discovery to bypass shortcomings of target-based drug design to yield a novel, non-lipogenic ABCA1 inducer with a beneficial metabolic profile yet without overt neutropenia or lipogenesis.

2. Methods

2.1. Synthesis of ethyl 3-(5-chloro-3-(N-(3,4-diethoxyphenyl)-N-methylsulfamoyl)thiophene-2-carboxamido)benzoate (CL2-57)

First, **1** (Fig. S1, 500 mg) was dissolved in THF, then triethylamine (203 mg) and **2** (363 mg) were added. Reaction was stirred overnight, after which solvent was removed under reduced pressure. Mixture was redissolved in EtOAc, washed with 1 N HCl and brine, then dried over Na_2SO_4. Solvent was removed under reduced pressure to yield **3**. Then, **3** (650 mg) was dissolved in N,N-DMF at 0°C. Sodium hydride (60% mineral oil dispersion, 124 mg) was added; reaction was stirred 30 min. Then, iodomethane (989 mg) was added; reaction was stirred overnight. Reaction was quenched with ice, then water and sodium hydroxide (150 mg) were added. Product was extracted with EtOAc, washed with brine, and dried over Na_2SO_4. Solvent was removed under reduced pressure to yield **4. 4** (630 mg) was dissolved in DCM, to which 1 drop N,N-DMF was added. Then, oxalyl chloride (381 mg) was added; reaction was heated to 40°C for 2 h. Solvent was removed under reduced pressure, with additional DCM added and removed (to azeotropically remove oxalyl chloride). Mixture was dissolved in DCM and added to a solution of ethyl 3-aminobenzoate (620 mg) and triethylamine (910 mg) in DCM; reaction was stirred overnight. Solvent was removed under reduced pressure, and the mixture was washed/dried as in the first step, then purified by recrystallization in diethyl ether and hexanes to yield CL2-57 as an off-white solid (600 mg, 58% overall yield, >99% purity). ^{1}H NMR (400 MHz, CDCl$_3$) δ = 1.29 (t, 3 H, J = 7.0 Hz), 1.37 (t, 3 H, J = 7.0 Hz), 1.43 (t, 3 H, J = 7.0 Hz), 3.23 (s, 3 H), 3.72 (q, 2 H, J = 7.0 Hz), 3.90 (q, 2 H, J = 7.0 Hz), 4.41 (q, 2 H, J = 7.0 Hz), 6.55−6.65 (m, 3 H), 7.30 (s, 1 H), 7.34 (t, 1 H, J = 8.0 Hz), 7.61 (ddd, 1 H, J_1 = 8.1 Hz, J_2 = 2.2 Hz, J_3 = 1.0 Hz), 7.80 (ddd, 1 H, J_1 = 7.9 Hz, J_2 = 2.5 Hz, J_3 = 1.2 Hz), 7.97 (t, 1 H, J = 1.9 Hz), 10.05 (s, 1 H). ^{13}C NMR (100 MHz, CDCl$_3$) δ = 14.5, 38.9, 61.1, 64.4, 112.5, 112.7, 119.1, 120.4, 123.7, 125.6, 125.7, 128.7, 130.1, 131.1, 131.8, 132.0, 135.3, 137.4, 142.6, 149.1, 149.2, 156.5, 166.0. LC-MS (*m/z*): calc. for $C_{25}H_{28}ClN_2O_7S_2$ [M + H$^+$]: 567.09, found: 567.0.

2.2. High-fat diet and drug treatment

C57Bl/6 male mice (Jackson Laboratories) were placed on HFD (60% kcal from fat, Envigo TD.06414) at 5 weeks. At 10 weeks, mice were acclimated to hydrogel replacement of drinking water (ClearH$_2$O) for 3 days. Then, for six weeks while HFD continued, mice received 10 mg/kg CL2-57 oral gavage Mon/Wed/Fri (vehicle: 9.5% PEG-200, 5% DMSO, 0.1% Tween-80 in water) plus 10 mg/kg/day CL2-57 in continuous hydrogel, or vehicle control. Mice were weighed weekly. For fast-refed studies, mice fasted for 16 h, then refed for 4 h. Blood glucose was measured with handheld glucometer. Sample size, chosen based on previous experience with glucose tolerance test, was ten mice per treatment. Mice were assigned to treatment groups by cage randomization upon arrival from Jackson. Mice were assigned a unique ear tag number to enable blinded tissue analysis and data collection. Treatment and *in vivo* experimentation were not blinded. No animals were excluded from analysis, and no control for confounders such as cage location or treatment order was performed.

2.3. Plasma/liver triglycerides

Blood was collected in EDTA-coated tubes (Microtainer K2E, BD) and centrifuged (3500 rpm, 15 min) to separate plasma. Livers were flash frozen in liquid nitrogen, then stored at −80 °C until

homogenization in isopropanol. Triglyceride levels were measured using reagents from Wako Diagnostics per manufacturer's protocol.

2.4. Glucose tolerance test (GTT)

After 16 h fast, animals were administered 1.5 g/kg body weight (bwt) glucose by intraperitoneal (*i.p.*) injection. Glucose in tail vein blood was measured at 0, 10, 20, 30, 45, 60, and 120 min using a One-Touch UltraMini glucometer (LifeScan, Inc). Additional blood was collected at multiple points between 0 and 30 min in heparinized capillary tubes and centrifuged, with plasma insulin levels determined by ELISA (ALPCO).

2.5. Neutrophil counts

CD1 mice (*n* = 5 per group) were administered T0901317, CL2-57, or vehicle at 10 mg/kg by oral gavage for three days. After final dose, blood samples were run on an Advia 120 analyzer (Bayer) for neutrophil counts.

2.6. Food intake

C57Bl/6 mice (*n* = 7, 2 M/5F) were housed in wire-bottom cages. After three days of acclimatization, all mice received oral gavage vehicle for four days followed by 10 mg/kg CL2-57 for four days. Food mass in cage was weighed before first gavage and again before/after food replenishment on each subsequent day to determine daily food intake. Each mouse acted as its own control in this treatment paradigm.

2.7. Insulin sensitivity studies

Mice were injected with 1 U/kg bwt Humalog insulin or vehicle (*n* = 3 of each per treatment group) 15 min before sacrifice. Liver, sub-cutaneous fat, and gastrocnemius were collected and homogenized in lysis buffer (50 mM Tris−HCl (pH 7.4), 100 mM NaCl, 1 mM EDTA, 1 mM EGTA, 1% Triton X-100, with protease/phosphatase inhibitor (Complete, Roche)). Protein concentration was determined using Bradford reagent (Bio-Rad). 30 μg denatured protein was separated by SDS-PAGE (Mini-PROTEAN TGX Gels 10%, Bio-Rad) and transferred to 0.45 μm nitrocellulose membranes. Membranes were blocked with 5% skim milk in TBST (1X TBS + 0.1% Tween-20) for 1 h, incubated with primary antibodies overnight at 4 °C, washed with TBST, and incubated with HRP-linked secondary antibodies for 1 h. After TBST wash, Clarity Western ECL Substrate (Bio-Rad) was added. Blots were imaged and analyzed using a ChemiDoc MP and Image Lab Ver 6.0 (Bio-Rad). Protein levels were normalized to GAPDH (muscle) or β-actin (liver, adipose) for quantification. Primary antibodies: Cell Signaling Technology 4060 (pS473Akt, RRID:AB_2,315,049) 13038 (pT308Akt, RRID:AB_2629447), 4691 (pan-Akt, RRID:AB_915783), 5174 (GAPDH, RRID:AB_10622025) and Sigma A2228 (β-actin, RRID: AB_476697).

2.8. Luciferase

HepG2 cells (RRID:CVCL_0027) purchased from ATCC and used without further validation were stably transfected with pGreen-Fire1-LXRE-in-ABCA1 plasmid, which contains ABCA1 promoter sequence linked to a luciferase response element, then selected over multiple generations with puromycin and frozen in liquid N$_2$. For assay, transfected cells were plated 24 h in media (Gibco) containing charcoal-stripped serum (Gemini), followed by 24 h treatment. Cells were lysed with passive lysis buffer (Promega),

frozen at −80°C for 15 min, and shaken at room temperature for 2 h before quantification with luciferase assay system (Promega) on Synergy Neo2 plate reader.

2.9. Cholesterol efflux

Plated J774 cells (RRID:CVCL_0358) purchased from ATCC and used without further validation were incubated in serum-free media containing 0.5 μM BODIPY-cholesterol (Cayman) for 24 h. Media was replaced with fresh serum-free media containing test compound for 24 h. For experiments with probucol (Sigma), it was added at 20 μM for the final 2 h with test compound. Then, fresh serum-free media containing 20 μg/mL purified recombinant apolipoprotein A1 (Sigma) was added for 6 h. Acceptor-containing media was transferred to a new plate, while cells were lysed with RIPA buffer. Fluorescence (Ex480/Em530) was measured in both components, with data reported as % efflux = (media fluorescence)/(media fluorescence + lysate fluorescence) normalized to background efflux (% efflux in DMSO-treated cells without exogenous apoA1).

2.10. qRT-PCR

For cell samples, treated cells were lysed with RLT plus lysis buffer (Qiagen). RNA was isolated with Qiagen RNEasy Plus columns per manufacturer instructions, then reverse transcribed to cDNA using SuperScript III (200 U/μL, Invitrogen) per supplier protocol. qPCR experiments were either performed with TaqMan gene expression master mix (Invitrogen) on a StepOne qPCR instrument or with PerfeCTa SYBR Green SuperMix (Quanta Biosciences) on CFX Connect Real-Time PCR Detection System (BioRad), with fold-change quantified by $\Delta\Delta C_t$. For animal samples, 100 mg tissue was homogenized in 1 mL TRIzol reagent (Ambion), mixed vigorously in chloroform, and separated by centrifugation. Aqueous layer containing RNA was added to Qiagen RNEasy Plus column; remaining steps were as described above for cell lysates.

qPCR primers. Below is a list of primers utilized for qPCR experiments.
TaqMan primers (ThermoFisher − Mm = mouse, Hs = human):
ActB: Mm01205647_g1, Hs99999903_m1
Gapdh: Hs02786624_g1
Hprt: Mm03024075_m1
Abca1: Mm00442646_m1, Hs02059118_m1
Abcg1: Mm00437390_m1
Abcg5: Mm00446241_m1
Ccl2: Mm00441242_m1
Cox2: Mm03294838_g1
Cxcl10: Mm00445235_m1
Cyp7a1: Mm00484150_m1
Il6: Mm00446190_m1
Irs1: Mm01278327_m1
Lpcat3: Mm00520147_m1
Nos2: Mm00440502_m1
Nr1h2: Mm00437265_g1
Nr1h3: Mm00443451_m1
Ppargc1a: Mm01208835_m1
Slc2a1: Mm00441480_m1
Srebf1: Mm00550338_m1, Hs01088691_m1
Tnf: Mm00443258_m1
Sybr green primers (all mouse):
18S   forward: CTCAACACGGGAAACCTCAC   reverse: AGACAAATCGCTCCAAC
Pck1   forward: TGGAAGGTCGAATGTGTGGG   reverse: AGCCCTTAAGTTGCCTTGGG

Ppara forward: GTATCTCACCGGGAGGCGTT reverse: CAGAGCGCTAAGCTGTGATG
G6pase forward: CCGGATCTACCTTGCTGCTC reverse: CACAGCAATGCCTGACAAGAC
Scd1 forward: ATCGCCCCTACGACAAGAAC reverse: GTTGATGTGCCAGCGGTACT

2.11. In vitro *immunoblot*

Cells were lysed with RIPA buffer (Sigma) containing protease/phosphatase inhibitors (Cocktails II and III, respectively, EMD Millipore). Protein was quantified by BCA assay (Thermo). Denatured proteins were separated by gel electrophoresis (NuPage 4−12% Bis-Tris, Invitrogen) in MOPS running buffer at 120 V for 1 h. Proteins were transferred to PDVF membranes (iBlot2). Membrane was blocked in 5% skim milk for 1 h, incubated with primary antibody at 4 °C overnight, washed with TBST, and then incubated with HRP-linked secondary antibody (Cell Signaling Technology) for 1 h at room temperature. After TBST wash, membrane was imaged using Supersignal West Femto substrate (Thermo Scientific) on Azure Biosystems c400 imager. Antibodies used: Abcam ab18180 (ABCA1, RRID: AB_444302), ThermoFisher MA5−11685 (SREBP1, RRID: AB_10984077), Invitrogen MA5−15738 (GAPDH, RRID: AB_10977387).

2.12. siRNA knockdown

J774 cells were plated in 24-well plates in serum-containing media, to which additional 100 μL media containing 10 pmol of siRNA and 3 μL of Lipofectamine RNAiMax reagent (ThermoFisher) were added. After 24 h, serum-free media containing 10 μM Cl2-57 or vehicle control was added to each well for 24 h. Cells were lysed and analyzed per qPCR and immunoblot procedures above. siRNAs used: Thermofisher 188,584 (Nr1h3 silencer), 186,947 (Nr1h2 silencer), and AM4611 (Silencer Negative Control siRNA #1).

2.13. NHRscan receptor binding assays

Nuclear hormone receptor was performed by DiscoverX (Fremont, CA) on their NHR-Scan platform of cell-based protein-protein interaction assays. This platform employs a β-gal reporter that activates upon interaction of full-length receptor protein with steroid coactivator receptor peptides. In agonist mode, activity of CL2-57 at 10 μM is compared to maximal activity of published positive control agonists; in antagonist mode, reduction in activity with 10 μM CL2-57 from that observed at EC_{80} of published agonists is quantified.

2.14. TR-FRET receptor binding assays

LanthaScreen TR-FRET coactivator assay kits for LXRβ (ThermoFisher A15129) and PPARγ (ThermoFisher PV4548) were performed according to manufacturer instructions using low-binding black 384-well plates and Synergy Neo2 plate reader. For the PPARγ assay, standardization was first performed with control agonist (pioglitazone), then run in two antagonist assays: dose-response of pioglitazone with or without a single concentration of CL2-57, and dose-response of CL2-57 cotreated with a single concentration (500 nM) pioglitazone. Each compound dose was performed in quadruplicate on each plate, and each experiment was performed in triplicate.

2.15. Global metabolomics

Liver and plasma samples were analyzed for global metabolomics profiling by Metabolon (Durham, NC) per their standard procedures, including extraction, detection via UPLC-MS/MS, quality control, and peak identification. Samples were blinded for analysis via bar code assignment by the authors before shipping to Metabolon. Principal components and hierarchical clustering analyses, visualization maps, and box-and-whisker plots were performed/produced by Metabolon.

2.16. Ethics

Experiments were approved by the UIC Animal Care Committee (protocol #16−106), which holds AALAAC accreditation (#000186) and OLAW assurance (#A3460.01).

2.17. Statistical analysis

In vitro experimentation was performed in minimum of biological triplicate, with technical replicates included in each assay plate/gel. Specifically, each assay utilized ≥3 separate plates of cells across different days, and each plate included ≥2 technical replicates of the same treatment. Sample sizes for animal experiments are indicated on each figure legend. Data visualization and statistical analysis (aside from metabolomics data) was performed in GraphPad Prism 8. $p<0.05$ was considered significant for all experiments; details of statistical tests for each experiment are provided in figure legends. All data were graphed as mean ± S.D.

2.18. Role of the funding source

No funding source had any role in study design; in the collection, analysis, and interpretation of data; in the writing of the report; or in the decision to submit the paper for publication. The corresponding author confirms that he had full access to all the data in the study and had final responsibility for the decision to submit for publication.

3. Results

3.1. Novel compound CL2-57 selectively induces ABCA1 and lessens inflammation in vitro

We screened a chemical library for selective inducers of ABCA1 versus SREBP1c, identifying hit compound F4 [25]. The lead compound, CL2-57, was synthesized (Fig. S1) as a chemically modified analog of F4. CL2-57 enhanced ABCA1-linked luciferase activity in HepG2 liver cells (E_{max} = 250% of vehicle; EC_{50} = 1.8 μM; Fig. S1b). Increased ABCA1 mRNA and protein were measured in HepG2 hepatocarcinoma (Fig. S1c) and J774 macrophage cell lines (Fig. S1d and e), with selectivity for *Abca1* over *Srebf1* induction demonstrated in HepG2 cells. In a fluorescent BODIPY-tagged cholesterol efflux assay [26], CL2-57 dose-dependently increased cholesterol efflux from macrophages to apoA1, the primary acceptor of cholesterol from ABCA1 *in vivo* (Fig. S1f) [27], and increased efflux was blocked by ABCA1 inhibitor probucol [28]. Stimulation of J774 cells with LPS increased TNFα and NOS2, modeling low-level inflammation that is chronically associated with T2D [29,30]; these increases were dose-dependently reversed by co-treatment with CL2-57 (Fig. S1g and h).

3.2. CL2-57 enhances glucose tolerance and insulin sensitivity in mice fed a high-fat diet

Male C57Bl/6 mice (Jackson) at five weeks were placed on a 60% kcal-from-fat diet for ten weeks and treated with vehicle or CL2-57 (*n* = 10/group) from weeks 5−10, per the following regimen: 10 mg/kg/day hydrogel, plus 10 mg/kg oral gavage every Monday, Wednesday, and Friday. This regimen, which mimics an extended release oral formulation, was chosen because of our previous success in utilizing hydrogel formulation to ensure continuous drug exposure and minimize stress from gavage [31,32]. Remaining hydrogel was measured to ensure consistent dosing.

Little change in fasting/refed glucose and insulin levels was observed with treatment initially (Fig. 1a and b). After five weeks, however, mice treated with CL2-57 showed improved performance in a glucose tolerance test (GTT). Drug-treated mice exhibited lower blood glucose concentrations following a single *i.p.* glucose injection, with total area under the curve during the 2-h test reduced by 20%

(Fig. 1c and d). These results were observed despite negligible change in insulin secretion during the first 20 min of the GTT (Fig. 1e).

To further investigate improvements in glucose handling, mice were administered *i.p.* insulin or vehicle 15 min before sacrifice (*n* = 3/group). Excised muscle, liver, and adipose homogenates were probed for phosphorylated (S473 or T308) and pan-Akt protein.
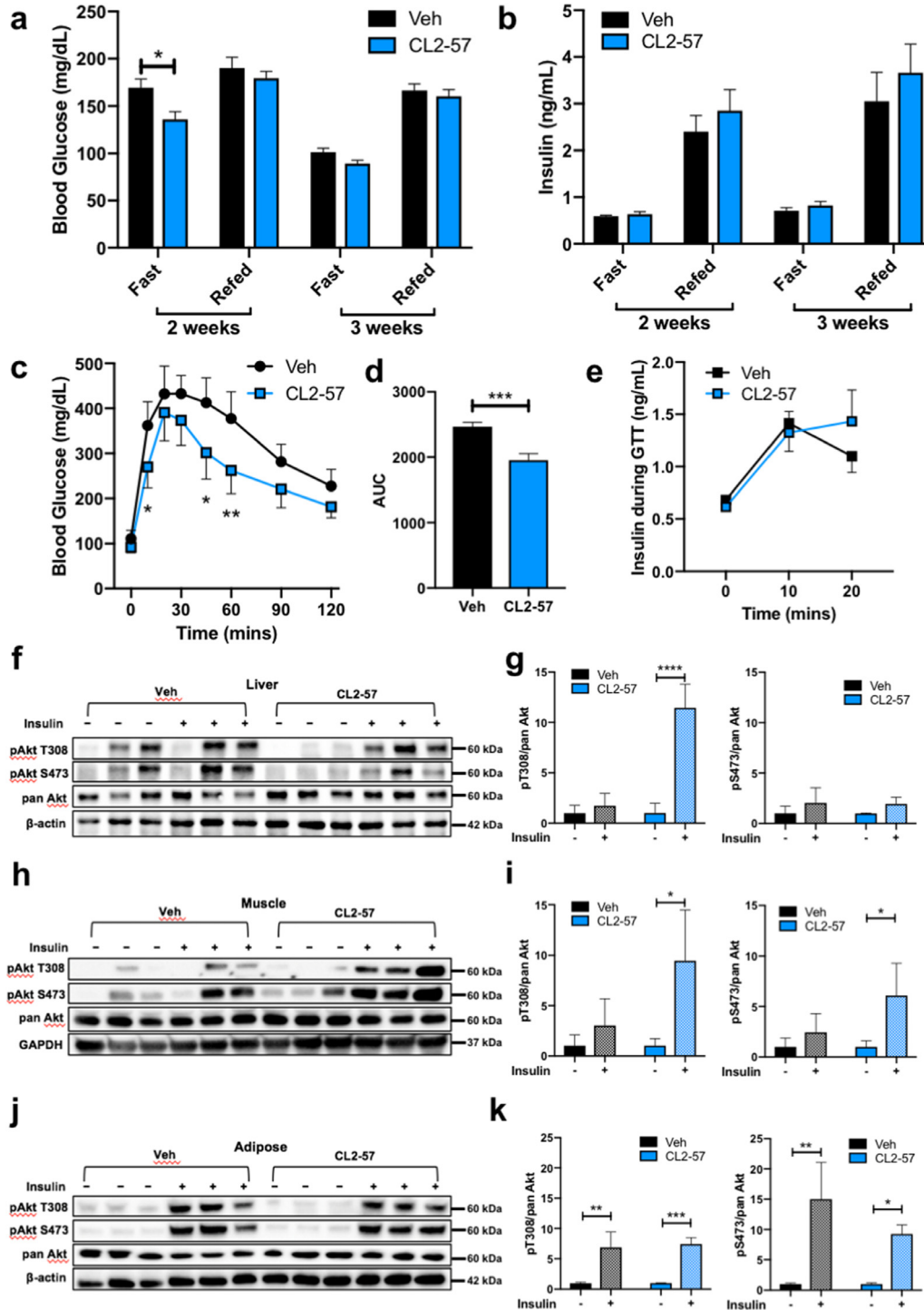
Fig. 1. Glucose homeostasis and insulin sensitivity with HFD and CL2-57. **a-b)** Plasma glucose (**a**) and insulin (**b**) levels after 16 h fast and 4 h refed periods. **c)** Glucose tolerance test demonstrating blood glucose levels from *t* = 0−120 min following single *i.p.* injection at *t* = 0. **d)** Total area under the curve during GTT. **e)** Insulin release during the first 20 min of the GTT. **f-k)** Representative immunoblot of mouse liver (f), muscle (h), and adipose (j) tissue homogenates for total Akt and forms phosphorylated at Thr308 and Ser473 following insulin challenge test, with accompanying densitometry analysis for liver (g), muscle (i) and adipose (k). Data is presented as mean ± S.D. for *n* = 9−10 mice per group for **a-e** and *n* = 3 per group for **g, i, k**. *$p<0.05$, **$p<0.01$, ***$p<0.001$, ****$p<0.0001$. Data analyzed by two-way ANOVA with post-hoc Sidak's multiple comparisons for differences between groups at each time point (**a-c, e**), by unpaired *t*-test (**d**), or by *t*-test with Dunnett's correction for multiple comparisons (**g, i, k**).

Increased phosphorylated:total Akt ratio in response to insulin correlates with tissue insulin sensitivity. Liver Akt phosphorylation at Thr308 increased with insulin in the CL2-57 group, while Ser473 did not change with insulin in either group (Fig. 1f and g). However, the strongest effect occurred in skeletal muscle, in which CL2-57 dramatically increased insulin sensitivity versus vehicle (Fig. 1h and i). No treatment effect occurred in adipose: Akt phosphorylation responded to insulin in both groups (Fig. 1j and k).

3.3. Weight gain and adiposity associated with HFD were reduced by CL2-57

Treatment with CL2-57 reduced weight gain from 17% to 8% of baseline over six weeks (Fig. 2a). Treatment also shifted tissue mass from fat to lean as measured by TD-NMR analysis (Fig. 2b), a technique that uses changes in water relaxivity induced by the surrounding environment to quantify fat and lean tissue mass. By combining body weights with NMR data, we determined that reduced weight gain was driven by reduced fat mass. On average, CL2-57-treated

mice actually gained lean tissue mass, suggesting that reduced weight gain was not driven by behavioral changes or compound toxicity, which was corroborated by follow-up food intake measurements (Fig. S2). White adipose tissue mass in both visceral (renal) and superficial (inguinal) fat pads was reduced by >20% proportional to body weight with CL2-57, with no change in brown adipose or liver mass (Fig. 2c). Despite negligible change in liver size, liver TGs were reduced by 35% with CL2-57, which was mirrored by a 25% decrease in plasma TGs (Fig. 2d).

We further investigated these findings at the transcriptional level in liver homogenates. As expected, *Abca1* expression increased with CL2-57 treatment along with ABCA1 protein (Figs. 2e and S3a); however, *Abcg1* was unchanged. Bile acid transport gene *Abcg5* was significantly reduced with CL2-57, and a diminishing trend was also observed with *Cyp7a1* mRNA, which encodes the rate-limiting step of bile acid synthesis [33]. We observed a small increase in *Srebf1* mRNA, consistent with *in vitro* data (Fig. 2f), as well as a corresponding increase in the uncleaved, endoplasmic reticulum form of SREBP1c protein (Fig. S3b) [34]. However, the mature, nuclear form
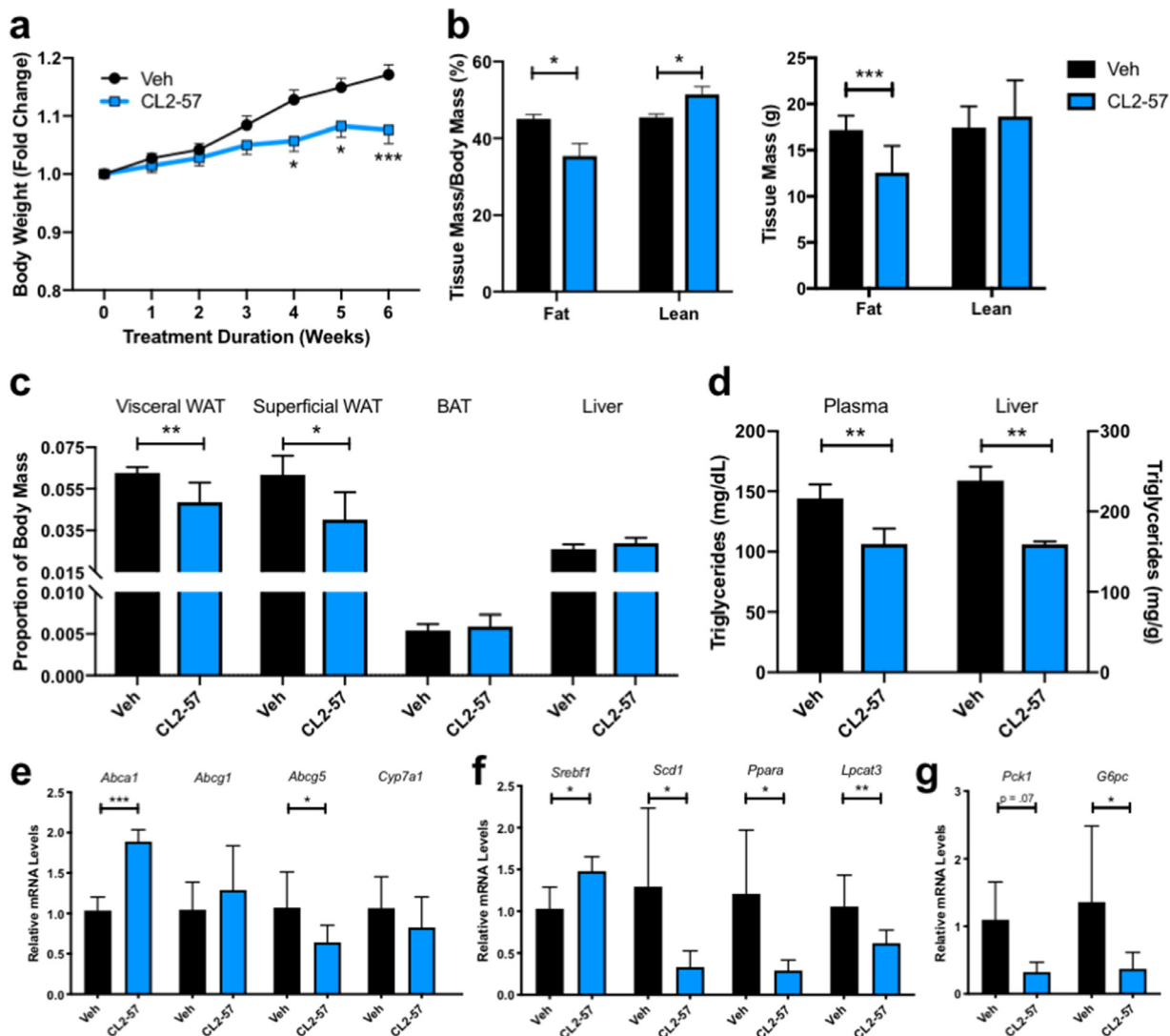
Fig. 2. Reduction in HFD-induced adiposity and alterations in liver gene expression with treatment. **a)** Weight gain associated with HFD and CL2-57 treatment. **b)** TD-NMR experiment to determine fat and lean tissue mass as a percentage of total body mass in treated mice (left). From percentages and body weights, absolute masses of fat and lean tissue in both groups was determined (right). **c)** White adipose tissue (renal and inguinal fat pads), brown adipose tissue, and liver mass as proportion of total body weight. **d)** Liver and plasma triglyceride concentrations in HFD mice with CL2-57 treatment. **e)** mRNA expression of sterol transport genes in liver tissue. **f)** mRNA expression of triglyceride metabolism-related genes in liver tissue. **g)** mRNA expression of gluconeogenic genes in liver tissue. All data is presented as mean ± S.D. for **a-d)** n = 9−10 mice per group and **e-g)** n = 4−6 mice per group. *p<0.05, **p<0.01, ***p<0.001 by unpaired t-test with Sidak's correction for multiple comparisons.

of SREBP1c protein was unchanged with treatment, and several additional genes related to fatty acid synthesis and metabolism, such as *Scd1* and *Lpcat3* were significantly reduced by CL2-57 in HFD mice. Expression of mRNA encoding the nuclear receptor PPARα, a key regulator of fatty acid metabolism, likewise fell 75%. Finally, *Pck1* and *G6pc*, which encode two key gluconeogenic enzymes, decreased by 70% and 73%, respectively, with CL2-57 (Fig. 2g).

3.4. Metabolomics identified gluconeogenesis and fatty acid metabolism as key pathways modulated by CL2-57 in HFD mice

To fully characterize the non-lipogenic ABCA1 inducer lead and complement phenotypic data, we performed global metabolomic profiling of mouse plasma and liver samples. HFD produced a robust phenotype: >50% of all detected metabolites varied with diet (Table 1). Principal components and hierarchical clustering analyses (Fig. S4a and b) illustrated this phenomenon, with close clustering by diet. Meanwhile, CL2-57 produced a broad treatment effect, impacting ~20% of measured metabolites. Table 1 highlights the diet-dependence of this effect, with 14% (plasma) and 19% (liver) of metabolites varying with diet-treatment interaction compared to 8% and 6% with treatment alone. Further illustrating diet-dependence, C57Bl/6 control mice receiving CL2-57 via daily *p.o.* treatments for one week (10 mg/kg, $n = 4$/group) showed no change in glucose or plasma free fatty acid metabolites, while low-magnitude increases in hepatic lipogenesis were observed (Fig. S5).

In contrast, in HFD mice, metabolomics identified several pathways modulated by CL2-57. Liver cholesterol, reduced in HFD mice (Fig. S4c), was normalized to baseline with treatment, as would be expected from a compound that increases ABCA1 expression and, therefore, RCT [35]. HFD reduced liver cholesterol yet increased downstream oxysterol metabolites, 7-hydroxycholesterol and 4-cholesten-3-one, which again was reversed with treatment (Fig. S4d and e). Levels of cholesterol and these metabolites in plasma were unaffected by CL2-57 (Fig. S4f−h).

Treatment with CL2-57 also reduced gluconeogenic metabolites. Increases of the four gluconeogenic precursors, in particular glutamine and glycerol, observed with HFD were attenuated by CL2-57 (Fig. 3a). A similar trend of HFD-induced increases corrected by CL2-57 was observed for key gluconeogenic/glycolytic intermediates, including liver glucose (Fig. 3b). These metabolomic data support the phenotypic readouts that we observed revealing improved glucose tolerance and insulin signaling and transcriptional data showing reduced gluconeogenic gene expression following treatment.

Finally, reduced adiposity and liver TG content of treated mice was corroborated by metabolomic profiling. HFD produced increases across nearly every lipid metabolite subclass in liver (Fig. S6a), with CL2-57 reversing many of these changes (Fig. S6b). These effects were particularly strong for free fatty acids (FFA), monoacylglycerols (MAG), and, to a lesser extent, diacylglycerols (Fig. 4a). Liver FFA levels in HFD mice ranged from 3−15x higher than normal diet mice; MAG increases with HFD versus normal diet ranged from 7−41x. CL2-57 reduced FFA concentrations from these increased levels by 40−90%; MAGs decreased 83−97% with CL2-57 compared to HFD alone. Plasma FFA and MAG levels were also increased by HFD, although only by <2−3x compared to normal diet (Fig. 4b). The effect of CL2-57 in reversing these increases was also muted in plasma (FFAs decreased 5−20%), suggesting a primary treatment effect in the liver.

3.5. CL2-57 broadly attenuated pro-inflammatory cytokines, enzymes, and metabolites in HFD mice

Plasma concentrations of arachidonic acid (AA), the three fatty acid AA precursors, and three downstream eicosanoids were increased with HFD, with those increases attenuated by CL2-57 (Fig. 5a). In particular, circulating AA increased 120% in HFD mice receiving vehicle, while HFD mice treated with CL2-57 experienced only a 37% increase over diet controls. Plasma levels of other proinflammatory lipid mediators − in particularly, lysophospholipids − followed a similar trend to AA metabolites. Increases up to 5x over normal diet were observed in HFD mice, along with 20−60% attenuation of those increases by CL2-57 treatment (Fig. 5b). We also profiled liver and adipose for proinflammatory enzymes (COX2 and NOS2), cytokines (TNFα and IL-6), and chemokines (CCL2 and CXCL10). Drug treatment substantially lowered mRNA levels of these markers, notably liver enzymes and chemokines and adipose TNFα (Fig. 5c). Additionally, NO precursors arginine and guanidinosuccinate were increased by HFD, an effect reversed by CL2-57 (Fig. S7a and b). The ketone body 3-hydroxybutyrate followed that same trend in plasma (Fig. S4c). Creatinine, urea, and bilirubin, which can serve as markers of global inflammation and/or organ toxicity, were unaffected by CL2-57 (Fig. S7d−f).

3.6. Target deconvolution identified CL2-57 as an LXRβ-selective agonist and PPAR/RXR antagonist

Target identification with cell-based β-gal reporter assays revealed that CL2-57 functioned as a partial LXR agonist, with 2.5-fold β/α selectivity by E_{max} (Fig. 6a), as well as a weak antagonist at RXRγ, PPARβ/δ, and PPARγ, supporting the hypothesis that phenotypic screening could identify compounds engaging multiple targets. Dose-response binding studies measuring coactivator recruitment via TR-FRET confirmed LXRβ agonism with $EC_{50} = 1.3$ μM, compared to 67 nM for T0901317 (Fig. S8a). Weak competitive antagonism of pioglitazone at PPARγ was also observed with CL2-57. Addition of 10 μM CL2-57 caused a 2.1-fold right-shift in the TR-FRET dose-response for pioglitazone ($p < 0.01$; Fig. S8b). At a constant pioglitazone concentration, CL2-57 again exhibited weak but significant antagonism (20−45% TR-FRET signal reduction) at concentrations ≥1 μM (Fig. S8c). The carboxylic acid derivative of CL2-57, which would be expected to form *in vivo* via ester hydrolysis, was inactive in all of the β-gal screens and in both TR-FRET binding assays (data not shown). A summary of *in vitro* data highlights the selectivity of CL2-57 for LXRβ/ABCA1 over LXRα/SREBP1c and its increasing efficacy versus T0901317 in assays of increasing biological complexity, from 75% in LXRβ binding to 183% in cholesterol efflux (Fig. 6b). While a phenotypic strategy is inherently challenging for mechanistic interpretation due to engagement of several targets, the importance of LXR agonism to *in vitro* activity of CL2-57 was further interrogated. Experiments employing siRNA knockdown (efficiency by qPCR: 38% for LXRα and 36% for LXRβ) demonstrated that the effect of CL2-57 on ABCA1 induction *in vitro* was mediated by LXRβ (Fig. 6c). Induction of both *Abcg1* and *Slc2a1* (GLUT1) by CL2-57 was also reduced by LXRβ knockdown, while *Irs1* increases were not affected by loss of

Table 1
Two-way ANOVA analysis of metabolomics data. Total number of detected metabolites in plasma and liver is indicated, along with number of metabolites that were significantly influenced by diet, CL2-57, or interaction between diet and treatment.

Plasma: 809 metabolites analyzed			
	Diet	Treatment	Interaction
Biochemicals $p<0.05$	469	61	115
Biochemicals $0.05<p<0.10$	64	51	70

Liver: 847 metabolites analyzed			
	Diet	Treatment	Interaction
Biochemicals $p<0.05$	400	51	162
Biochemicals $0.05<p<0.10$	62	44	73
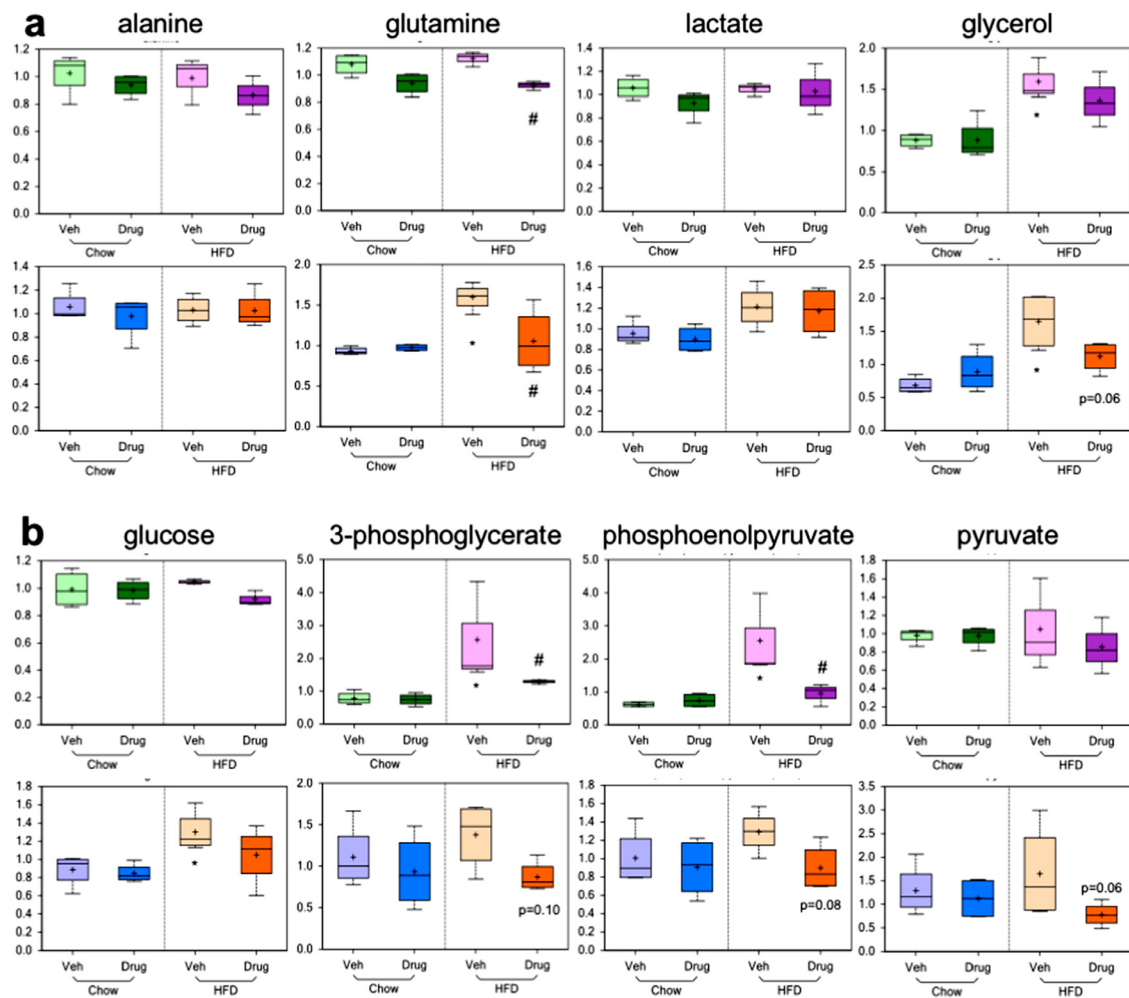
Fig. 3. Decreases in liver gluconeogenesis illustrated by metabolomic analysis. **a)** Plasma (top) and liver (bottom) levels of the four primary gluconeogenic substrates are shown. **b)** Plasma (top) and liver (bottom) levels of key glycolytic/gluconeogenic intermediates are shown. Data presented as mean (+ sign), median (center line), interquartile range (shaded area), and range (error bars) for $n = 4$ per group. $^*p < 0.05$ vs. chow-veh, $^\#p < 0.05$ vs. HFD-veh by unpaired t-test.

either LXR isoform (Fig. S8d−f). Meanwhile, LXR target gene *Apoe* was not significantly affected by CL2-57 treatment in J774 cells (Fig. S8g). Finally, ABCA1-linked luminescence increased (from 2.5- to 4.5-fold) with CL2-57 titration in the presence of RXR agonist bexarotene; however, no increase was observed when CL2-57 was titrated in the presence of pan-LXR agonist T0901317 (Fig. S8h). Having detected LXR agonist activity with CL2-57, we treated CD1 mice to evaluate for known adverse effects of LXR agonists. Three daily *p.o.* treatments with CL2-57 did not affect plasma TG or cholesterol, nor circulating neutrophil levels (n = 5/group), whereas T0901317 increased TG and reduced neutrophils (Fig. 6d and e). In a supplemental study, C57Bl/6 mice treated for one week with daily *p.o.* CL2-57 also experienced no changes in plasma TG or cholesterol compared to vehicle controls (Fig. 6f).

4. Discussion

The phenotypic drug discovery strategy presented herein focused on a non-lipogenic ABCA1 inducer that elevated *Abca1* selectively over *Srebf1* in liver cells. Underlying this strategy was the desire to gain beneficial effects in T2D without unwanted hepatic lipogenesis and, in particular, to test a phenotypic alternative to biochemical optimization of LXRβ agonists, an approach that, to date, has not translated to the clinic. In HFD mice, the test compound, CL2-57, showed beneficial, pleiotropic effects, highlighting the power of phenotypic drug discovery. Prior studies have identified suppression of

gluconeogenesis as a key mechanism underlying improved insulin sensitivity with an LXR agonist [4], which was also observed with CL2-57. Direct effects of LXR agonism on insulin signaling in skeletal muscle, which, unlike liver and white adipose, expresses only the LXRβ isoform, have also been reported [20], corroborating our insulin challenge data that identified muscle as a key site of enhanced Akt phosphorylation with treatment. Finally, LXR agonists are anti-inflammatory, both through direct transrepression of proinflammatory genes and indirect signaling disruption via ABCA1-mediated cholesterol mobilization and reduction in membrane cholesterol [19,21]. With CL2-57, we similarly observed broad reductions in proinflammatory enzymes, cytokines/chemokines, and lysophospholipids [36]. The observed anti-inflammatory effect of CL2-57 may reflect an important mechanism of action for non-lipogenic ABCA1 inducers in T2D beyond direct effects on glucose/insulin [37]. Together, our data reveal that while CL2-57 binds to nuclear receptor targets in addition to LXRβ, it reproduces many of the beneficial effects that have previously been observed with LXR agonists in T2D models.

We previously observed HDL-C increases with the original hit compound F420, from which CL2-57 was derived [25]. In the present study, CL2-57 was observed to increase levels of cholesterol in liver in HFD mice, compatible with enhanced RCT to the liver. However, short-term treatments of mice on normal chow, with either the test compound or control LXR agonist T0901317, demonstrated no effect on HDL-C levels. Several studies with T0901317 or GW3965 in WT or
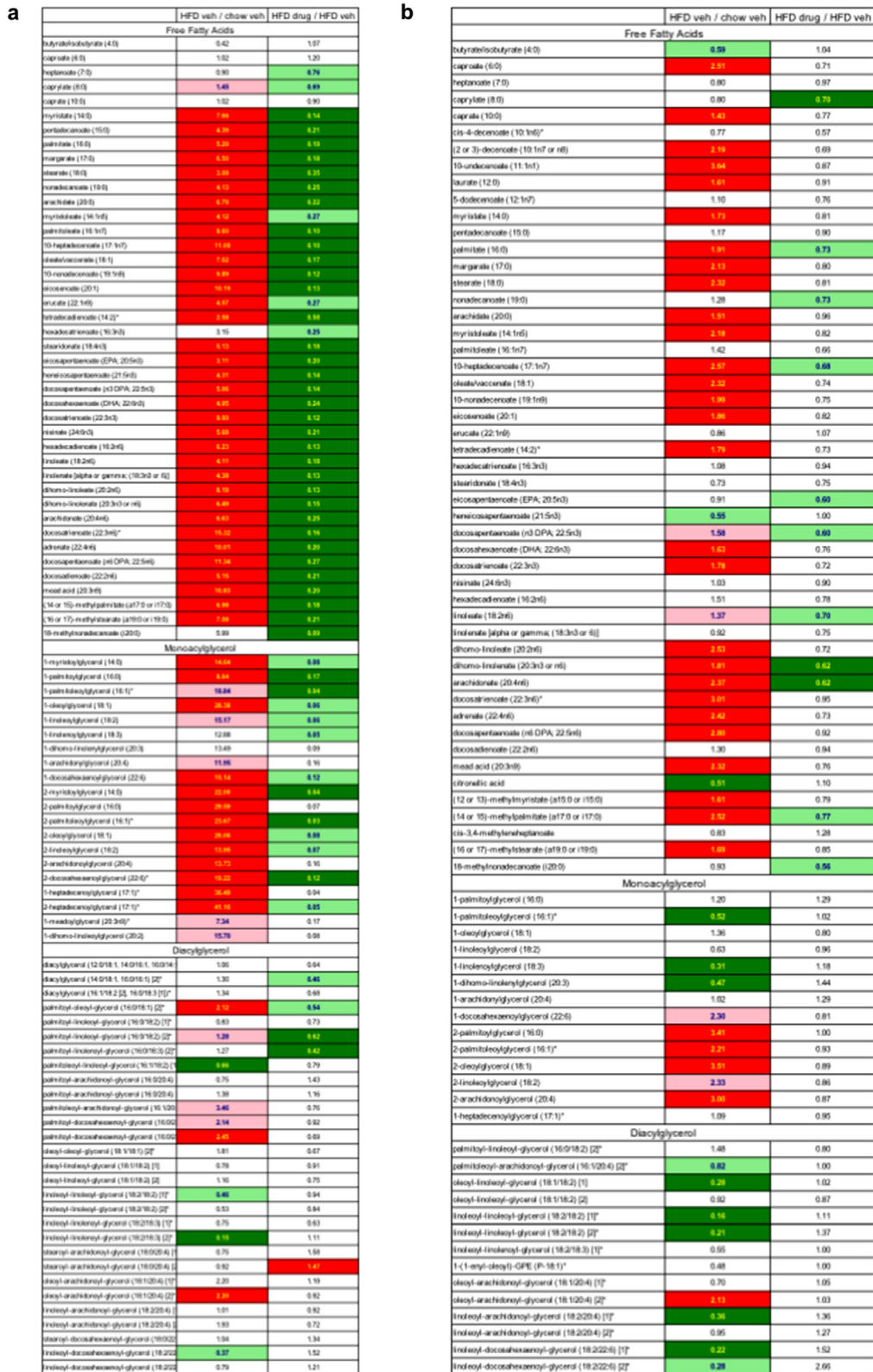
Fig. 4. Free fatty acid, monoacylglycerol, and diacylglycerol metabolite changes with HFD and CL2-57 treatment in liver (a) and plasma (b). Middle column indicates fold change in HFD vs. normal chow mice, and right column shows fold change with CL2-57 vs. vehicle in HFD mice. Data presented as mean of n = 3−4 per group. Bold red and green shading indicate increase or decrease, respectively, with $p < 0.05$. Pale shading represents $0.05 < p < 0.10$.

disease-model mice have reported increased ABCA1 expression and phenotypic efficacy, without changes in plasma HDL-C [2,38]. Moreover, the association between HDL and cardiovascular disease outcomes is complex and controversial [39]. The lack of increase in HDL-C in short-term treatment of mice on normal chow does not diminish the overall impact of CL2-57 on reversing HFD phenotypes.

Global metabolomics provided additional detail and context to standard *in vivo* readouts and enabled a qualitative comparison of
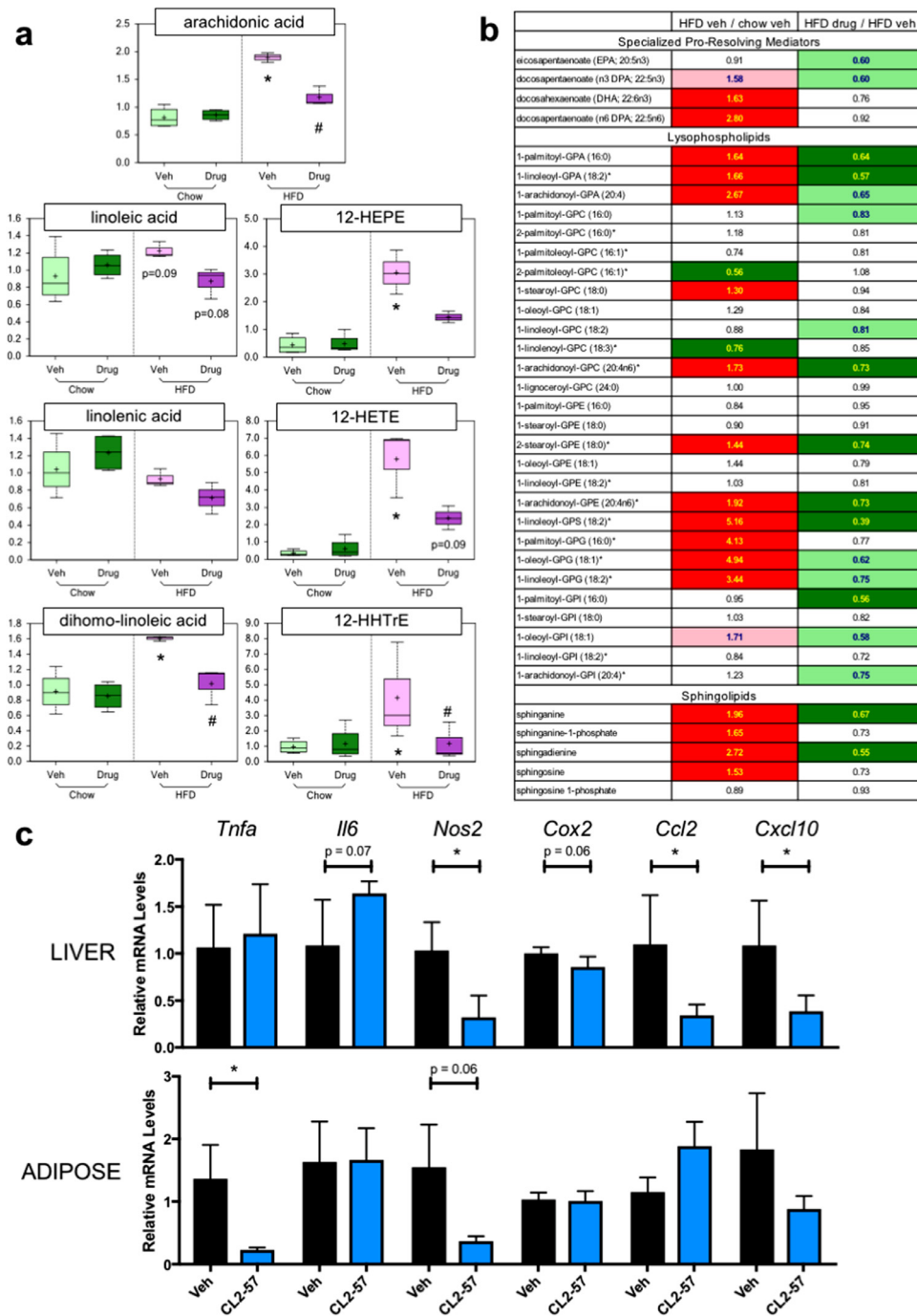
Fig. 5. Reduction in HFD-induced inflammatory lipid mediators and pro-inflammatory enzymes, cytokines, and chemokines with CL2-57. a) Change in plasma level of arachidonic acid (AA, top), upstream fatty acid AA precursors (left), and eicosanoids downstream of AA (right) with HFD and CL2-57. $*p < 0.05$ vs. chow-veh, $^{\#}p < 0.05$ v. HFD-veh by unpaired t-test. Data presented as mean (+ sign), median (center line), interquartile range (shaded area), and range (error bars) for $n = 4$ per group. b) Changes in plasma levels of additional immunomodulatory lipid metabolites with HFD and CL2-57 treatment are shown. Middle column represents fold change with HFD vs. normal chow, while right column represents fold change with CL2-57 vs. vehicle in HFD mice. Bold red and green shading indicate increase or decrease, respectively, with $p < 0.05$. Pale shading represents $0.05 < p < 0.10$. Data presented as mean for $n = 4$ per group. c) Changes in mRNA expression of various proinflammatory cytokines, enzymes, and chemokines in liver (top) and adipose (bottom) with CL2-57 vs. vehicle treatment in HFD mice. Data presented as mean $\pm$ S.D. for $n = 4-6$ per group, with $*p < 0.05$ by unpaired t-test.

CL2-57 to three other diabetes drugs for which metabolomics has been published: rosiglitazone, pioglitazone, and metformin (Table 2), using results summarized from seven publications [40−46]. CL2-57 offers potential improvement over the two thiazolidinediones through reduction of hepatic lipogenesis. Meanwhile, increased β-oxidation (i.e. acyl carnitine and ketone bodies) of lipids and reduced branched-chain amino acids are key metabolic effects of metformin not shared by CL2-57. However, we speculate that significant reductions in lipogenesis with our ABCA1 inducer may provide

complementary efficacy in combination treatment with metformin. Overall, metabolomic profiling is an uncommonly employed technique in preclinical drug development, but, in this study, it yielded important additional data to characterize the phenotype elicited by CL2-57 treatment in the HFD model and provided novelty compared to previous reports describing nuclear receptor ligands that focused solely on traditional readouts.

This study characterizing a non-lipogenic ABCA1 inducer represents a significant advancement over existing ABCA1 inducers
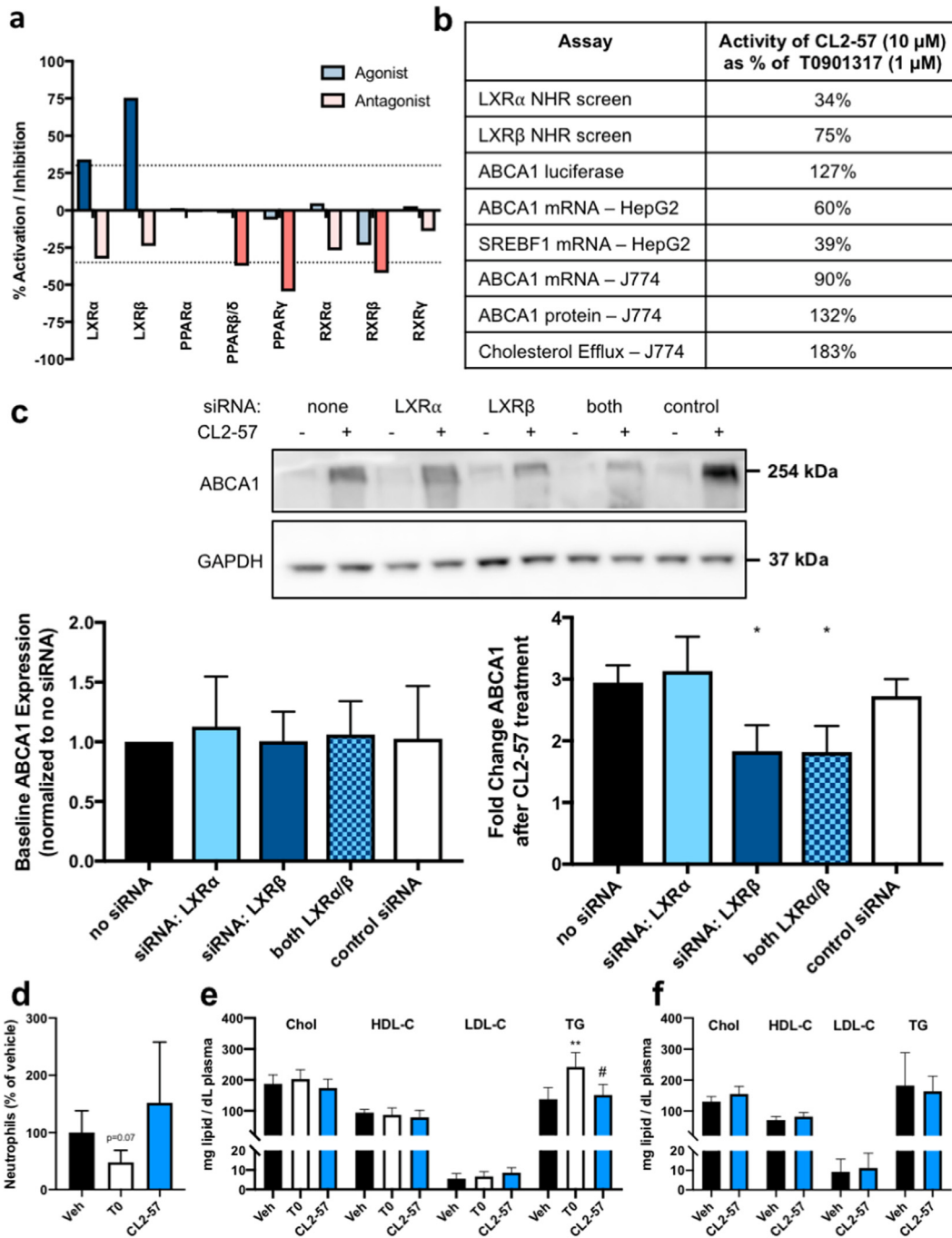
Fig. 6. Target deconvolution of CL2-57. **a)** Partial agonism of LXRβ and LXRα, per DiscoverX NHR screening assays, with weak antagonist activity at PPAR and RXR isoforms also observed. "Agonist" mode represents activity of 10 μM CL2-57 compared to maximum response of literature agonist. "Antagonist" mode represents % reduction in activity due to addition of 10 μM CL2-57 in presence of literature agonist at EC$_{80}$. Dashed line indicates significance threshold defined by DiscoverX. **b)** Summary of various *in vitro* assays performed as shown in Fig. S1 comparing the response produced by 10 μM CL2-57 to that induced by 1 μM T0901317. **c)** Effect of siRNA knockdown of LXR isoforms on baseline ABCA1 expression (left) and on response of ABCA1 expression to CL2-57. Representative image is shown, along with mean $\pm$ S.D. of densitometry analysis with three biological replicates. *$p<0.05$ vs. no siRNA treatment by one-way ANOVA with Dunnett's multiple comparisons test. **d)** Absolute neutrophil count (normalized to vehicle) in CD1 mice after three days *p.o.* treatment with T0901317, CL2-57, or vehicle. **e-f)** Plasma total cholesterol, HDL cholesterol, LDL cholesterol, and triglycerides (TG) in CD1 mice after three days *p.o.* treatment with 10 mg/kg T0901317, CL2-57, or vehicle (**e**) and C57Bl/6 mice after seven days *p.o.* treatment with CL2-57 or vehicle (**f**). Data presented as mean $\pm$ S.D. ($n = 5$ per group), with **$p<0.01$ vs. veh and #$p<0.05$ vs. T0 by one-way ANOVA with Tukey's multiple comparisons test.

(primarily LXR agonists) as potential treatments for T2D and related cardiometabolic syndrome. While GW3965 was initially posited as a selective option compared to T0901317 [47], subsequent studies revealed similar SREBP1c/TG increases [48,49]. Optimization of LXRβ-selective agonists for high affinity binding with 10−100x selectivity over LXRα is achievable [50]. However, biochemical assays with the truncated LXR ligand-binding domain used to optimize agonists do not directly correlate with transcriptional data. Ligand binding to

LXR stabilizes and derepresses a multi-protein complex, but transcriptional output (e.g. *Abca1* or *Srebf1*) depends on selective coregulator binding, which varies with the specific cellular context and ligand [49,51]. Efforts to identify ABCA1-inducing compounds have been made; however, these have involved either apoE-induction and avoiding lipogenesis by triaging LXR agonists [52,53], or focused development of LXR agonists [54,55]; moreover, *in vivo* studies are lacking. Our work provides a first *in vivo* proof-of-concept for

Table 2

Comparison of CL2-57 to metformin and thiazolidinediones in HFD metabolomics studies. Summary of published metabolomics data on response of various diet-induced rodent models of diabetes to metformin and thiazolidinedione (rosiglitazone or pioglitazone) treatment, in comparison to data collected in our study.

	Metformin		Thiazolidinediones		CL2-57	
	Liver	Plasma	Liver	Plasma	Liver	Plasma
ketone bodies	↑↑	↑↑	n.d.	n.d.	↔	↓↓
BCAA	n.d.	↓↓	↔	↓↓	↔	↔
triglycerides	n.d.	n.d.	↑↑	↓↓	↓↓	↓↓
free fatty acids	↓↓	n.d.	↑↑	↓↓	↓↓	↔
acyl carnitines	n.d.	↑↑	n.d.	n.d.	↔	↔
lysophospholipids	n.d.	↑↑	↑↑	n.d.	↓↓	↓↓

discovery and development of a non-lipogenic ABCA1 inducer that beneficially modifies T2D pathophysiology.

Differentiation of our ABCA1 inducer from classical LXR agonists can be seen in the observed reduction in adiposity and both liver and plasma TGs. T0901317 rapidly induces robust TG increases [2], while a study with GW3965 reported an adipose shift from visceral to subcutaneous depots as a potential beneficial effect [56]. By comparison, we observed decreased TG and reduced adipose at both sites. Corroborating these findings were reduced liver expression of key nuclear receptor target genes involved in lipogenesis, such as *Scd1* and *Lpcat3*, and accompanying decreases in fatty acid and monoacylglycerol metabolite levels with CL2-57. T0901317 and other classical LXR agonists strongly upregulate the entire lipogenic axis, including *Srebf1*, *Scd1*, and *Lpcat3*, which results in greatly enhanced triglyceride production and liver steatosis.

Of potential mechanisms explaining the distinct effects of our non-lipogenic ABCA1 inducer versus classical LXR agonists, we favor the dual agonist/antagonist mechanism of CL2-57 at LXRβ and PPARγ. This mechanism has literature and clinical precedent: fenofibrate is also proposed to elicit beneficial effects through dual agonist/antagonist activity at PPARα and LXRα [57]. The dual mechanism may underlie the altered fatty acid metabolism induced by CL2-57 compared to simple LXR agonists, as RXR and PPARγ antagonists have been found to decrease liver and adipose TGs in HFD mice, and *Scd1* is a target gene for PPARγ as well as LXR/SREBP1c [58]. Furthermore, genetic ablation of PPARα prevents SREBP1c-dependent transcriptional activation of *Scd1* and *Fasn*; thus, PPARα is necessary for an intact lipogenic axis extending from LXRα/SREBP1c transcription factors to downstream enzymes [59]. Notably, liver PPARα expression was reduced by >80% with CL2-57 treatment, which would be expected to disrupt lipogenesis similarly to genetic downregulation. These arguments support the dual agonist/antagonist mechanism of CL2-57.

The relationship of PPARγ with insulin resistance is complex because PPAR$\gamma^{-/+}$ heterozygotes manifest insulin resistance in response to PPARγ antagonists [60]. Thus, while either LXRβ or PPARγ activation can elicit anti-diabetes efficacy, it would seem that intact signaling at both LXRα and various PPAR isoforms is critical for hepatic lipogenesis. Unfortunately, mechanistic interrogation of this hypothesis with CL2-57 in LXR and PPAR knockout mice is a challenge, as these mice are resistant to HFD-induced obesity [61,62]. This resistance itself reflects the critical role of both nuclear receptors in lipogenesis.

Of further mechanistic relevance is the reduction of liver *Lpcat3* expression caused by CL2-57 treatment. *Lpcat3,* a target gene for both LXR and PPAR transcription factors, is a primary regulator of membrane phospholipid remodeling. By modifying liver phospholipids available for release in lipoproteins, LPCAT3 downregulation would contribute to the reductions in plasma polyunsaturated fatty acids (PUFA) and PUFA-containing lysophospholipids which we observed through metabolomic profiling [63,64]. Altered membrane lipid composition due to change in LPCAT3 also indirectly influences SREBP1c processing in the endoplasmic reticulum. Specifically, reduced *Lpcat3* expression correlates with reduced SREBP1c cleavage and, subsequently, reduced levels of the mature, nuclear SREBP1c protein required to promote lipogenesis [65]. Thus, the mechanisms discussed in the foregoing paragraphs would be sufficient to negate any effects resulting from the observed modest increase in *Srebf1* mRNA induced by CL2-57.

In conclusion, through functional, biochemical, and metabolomic analysis, we determined that CL2-57 attenuated pathologic HFD-induced phenotypes. Notably, treatment reduced HFD-induced weight gain, shifted fatty to lean tissue mass, reduced adiposity and plasma/liver TGs, and diminished inflammation. This multifunctional correction of T2D pathophysiology was complemented by positive safety readouts in HFD and non-HFD mice. Specifically, known LXR-mediated side effects of hypertriglyceridemia and neutropenia were avoided, and general toxicity markers were not elevated with treatment. Overall, oral delivery of a non-lipogenic ABCA1 inducer provided an efficacious and tolerated treatment in mice.

4.1. Caveats and limitations

Further studies are needed to confirm the dual agonist/antagonist mechanism of CL2-57. As we continue to optimize further derivatives with more potent LXRβ agonism, this effort will become important to delineate beneficial versus undesired effects for type 2 diabetes and related conditions. A further challenge in translating these results to the clinic will be to address the important distinctions between rodent and human metabolism regarding the role of LXR in lipid physiology. Specifically, mice lack the plasma cholesteryl ester transport protein (CETP) that exists in humans and is transcriptionally regulated by LXRα [66], while the inducible degrader of LDL (IDOL) protein also is differentially affected by LXR in rodents vs. humans [67]. Human iPSC-derived cell lines and other models of human physiology will be needed in tandem with non-human preclinical models.

Declaration of Interests

Contributors

Literature search and study design: C.T.L, M.W.K., M.B.A., M.J.L., B.T.L., and G.R.J.T; data collection: C.T.L, M.W.K., O.D., and M.A.B.; data interpretation: C.T.L, M.W.K., B.T.L, G.R.J.T; figures: C.T.L; writing – original draft: C.T.L; writing – review & editing: C.T.L, M.W.K., M.B.A., B.T.L., and G.R.J.T.; project supervision: M.J.L, B.T.L., and G.R.J.T. Funding acquisition: C.T.L, B.T.L., and G.R.J.T. All authors have read and approved the final version of this manuscript.

Funding

Acknowledgments

Data sharing statement

Novel compound CL2-57 generated in this study is available from the corresponding author with a completed Materials Transfer Agreement. Metabolomics dataset is available at http://dx.doi.org/10.17632/k2v8n7txry.1. Additional details on DiscoverX and Metabolon procedures are available from the corresponding author upon reasonable request.

Supplementary materials

Supplementary material associated with this article can be found, in the online version, at doi:10.1016/j.ebiom.2021.103287.

References

[1] Gao M, Liu D. The liver X receptor agonist T0901317 protects mice from high fat diet-induced obesity and insulin resistance. AAPS J 2013;15(1):258–66.

[2] Chisholm JW, Hong J, Mills SA, Lawn RM. The LXR ligand T0901317 induces severe lipogenesis in the db/db diabetic mouse. J Lipid Res 2003;44(11):2039–48.

[3] He Q, Pu J, Yuan A, Yao T, Ying X, Zhao Y, et al. Liver X receptor agonist treatment attenuates cardiac dysfunction in type 2 diabetic db/db mice. Cardiovasc Diabetol 2014;13:149.

[4] Commerford SR, Vargas L, Dorfman SE, Mitro N, Rocheford EC, Mak PA, et al. Dissection of the insulin-sensitizing effect of liver X receptor ligands. Mol Endocrinol 2007;21(12):3002–12.

[5] Archer A, Laurencikiene J, Ahmed O, Steffensen KR, Parini P, Gustafsson JA, et al. Skeletal muscle as a target of LXR agonist after long-term treatment: focus on lipid homeostasis. Am J Physiol Endocrinol Metab 2014;306(5):E494–502.

[6] Beaven SW, Matveyenko A, Wroblewski K, Chao L, Wilpitz D, Hsu TW, et al. Reciprocal regulation of hepatic and adipose lipogenesis by liver X receptors in obesity and insulin resistance. Cell Metab 2013;18(1):106–17.

[7] Laffitte BA, Chao LC, Li J, Walczak R, Hummasti S, Joseph SB, et al. Activation of liver X receptor improves glucose tolerance through coordinate regulation of glucose metabolism in liver and adipose tissue. Proc Natl Acad Sci USA 2003;100 (9):5419–24.

[8] Quinet EM, Savio DA, Halpern AR, Chen L, Miller CP, Nambi P. Gene-selective modulation by a synthetic oxysterol ligand of the liver X receptor. J Lipid Res 2004;45(10):1929–42.

[9] Forcheron F, Cachefo A, Thevenon S, Pinteur C, Beylot M. Mechanisms of the triglyceride- and cholesterol-lowering effect of fenofibrate in hyperlipidemic type 2 diabetic patients. Diabetes 2002;51(12):3486–91.

[10] Key CC, Liu M, Kurtz CL, Chung S, Boudyguina E, Dinh TA, et al. Hepatocyte ABCA1 deletion impairs liver insulin signaling and lipogenesis. Cell Rep 2017;19 (10):2116–29.

[11] Storti F, Klee K, Todorova V, Steiner R, Othman A, van der Velde-Visser S, et al. Impaired ABCA1/ABCG1-mediated lipid efflux in the mouse retinal pigment epithelium (RPE) leads to retinal degeneration. Elife 2019;8.

[12] Liu P, Peng L, Zhang H, Tang PM, Zhao T, Yan M, et al. Tangshen formula attenuates diabetic nephropathy by promoting ABCA1-mediated renal cholesterol efflux in db/db mice. Front Physiol 2018;9:343.

[13] Shao C, Tang C, Sinha A, Mayer PS, Davenport GD, Brot N, et al. Humans with atherosclerosis have impaired ABCA1 cholesterol efflux and enhanced high-density lipoprotein oxidation by myeloperoxidase. Circ Res 2014;114(11):1733–42.

[14] Fitz NF, Cronican AA, Saleem M, Fauq AH, Chapman R, Lefterov I, et al. Abca1 deficiency affects Alzheimer's disease-like phenotype in human ApoE4 but not in ApoE3-targeted replacement mice. J Neurosci 2012;32(38):13125–36.

[15] van Eck M, Bos IS, Kaminski WE, Orso E, Rothe G, Twisk J, et al. Leukocyte ABCA1 controls susceptibility to atherosclerosis and macrophage recruitment into tissues. Proc Natl Acad Sci USA 2002;99(9):6298–303.

[16] Westerterp M, Bochem AE, Yvan-Charvet L, Murphy AJ, Wang N, Tall AR. ATP-binding cassette transporters, atherosclerosis, and inflammation. Circ Res 2014;114(1):157–70.

[17] Bi X, Vitali C, Cuchel M. ABCA1 and Inflammation: from animal models to humans. Arterioscler Thromb Vasc Biol 2015;35(7):1551–3.

[18] Bochem AE, van der Valk FM, Tolani S, Stroes ES, Westerterp M, Tall AR. Increased systemic and plaque inflammation in ABCA1 mutation carriers with attenuation by statins. Arterioscler Thromb Vasc Biol 2015;35(7):1663–9.

[19] Ito A, Hong C, Rong X, Zhu X, Tarling EJ, Hedde PN, et al. LXRs link metabolism to inflammation through Abca1-dependent regulation of membrane composition and TLR signaling. Elife 2015;4:e08009.

[20] Baranowski M, Zabielski P, Blachnio-Zabielska AU, Harasim E, Chabowski A, Gorski J. Insulin-sensitizing effect of LXR agonist T0901317 in high-fat fed rats is associated with restored muscle GLUT4 expression and insulin-stimulated AS160 phosphorylation. Cell Physiol Biochem 2014;33(4):1047–57.

[21] Schulman IG. Liver X receptors link lipid metabolism and inflammation. FEBS Lett 2017;591(19):2978–91.

[22] Cannon MV, van Gilst WH, de Boer RA. Emerging role of liver X receptors in cardiac pathophysiology and heart failure. Basic Res Cardiol 2016;111(1):3.

[23] Schultz JR, Tu H, Luk A, Repa JJ, Medina JC, Li L, et al. Role of LXRs in control of lipogenesis. Genes Dev 2000;14(22):2831–8.

[24] Kirchgessner TG, Sleph P, Ostrowski J, Lupisella J, Ryan CS, Liu X, et al. Beneficial and adverse effects of an LXR agonist on human lipid and lipoprotein metabolism and circulating neutrophils. Cell Metab 2016;24(2):223–33.

[25] Ben Aissa M, Lewandowski CT, Ratia KM, Lee SH, Layden BT, LaDu MJ, et al. Discovery of nonlipogenic ABCA1 inducing compounds with potential in Alzheimer's disease and Type 2 diabetes. ACS Pharmacol Transl Sci 2021;4(1):143–54.

[26] Sankaranarayanan S, Kellner-Weibel G, de la Llera-Moya M, Phillips MC, Asztalos BF, Bittman R, et al. A sensitive assay for ABCA1-mediated cholesterol efflux using BODIPY-cholesterol. J Lipid Res 2011;52(12):2332–40.

[27] Phillips MC. New insights into the determination of HDL structure by apolipoproteins: thematic review series: high density lipoprotein structure, function, and metabolism. J Lipid Res 2013;54(8):2034–48.

[28] Wu CA, Tsujita M, Hayashi M, Yokoyama S. Probucol inactivates ABCA1 in the plasma membrane with respect to its mediation of apolipoprotein binding and high density lipoprotein assembly and to its proteolytic degradation. J Biol Chem 2004;279(29):30168–74.

[29] Creely SJ, McTernan PG, Kusminski CM, Fisher f M, Da Silva NF, Khanolkar M, et al. Lipopolysaccharide activates an innate immune system response in human adipose tissue in obesity and type 2 diabetes. Am J Physiol Endocrinol Metab 2007;292(3):E740–7.

[30] Kheder RK, Hobkirk J, Stover CM. In vitro modulation of the LPS-induced proinflammatory profile of hepatocytes and macrophages- approaches for intervention in obesity? Front Cell Dev Biol 2016;4:61.

[31] Tai LM, Koster KP, Luo J, Lee SH, Wang YT, Collins NC, et al. Amyloid-beta pathology and APOE genotype modulate retinoid X receptor agonist activity in vivo. J Biol Chem 2014;289(44):30538–55.

[32] Luo J, Lee SH, VandeVrede L, Qin Z, Piyankarage S, Tavassoli E, et al. Re-engineering a neuroprotective, clinical drug as a procognitive agent with high in vivo potency and with GABAA potentiating activity for use in dementia. BMC Neurosci 2015;16:67.

[33] Zhang L, Huang X, Meng Z, Dong B, Shiah S, Moore DD, et al. Significance and mechanism of CYP7a1 gene regulation during the acute phase of liver regeneration. Mol Endocrinol 2009;23(2):137–45.

[34] Owen JL, Zhang Y, Bae SH, Farooqi MS, Liang G, Hammer RE, et al. Insulin stimulation of SREBP-1c processing in transgenic rat hepatocytes requires p70 S6-kinase. Proc Natl Acad Sci USA 2012;109(40):16184–9.

[35] Attie AD, Kastelein JP, Hayden MR. Pivotal role of ABCA1 in reverse cholesterol transport influencing HDL levels and susceptibility to atherosclerosis. J Lipid Res 2001;42(11):1717–26.

[36] Sevastou I, Kaffe E, Mouratis MA, Aidinis V. Lysoglycerophospholipids in chronic inflammatory disorders: the PLA(2)/LPC and ATX/LPA axes. Biochim Biophys Acta 2013;1831(1):42–60.

[37] Tsalamandris S, Antonopoulos AS, Oikonomou E, Papamikroulis GA, Vogiatzi G, Papaioannou S, et al. The role of inflammation in diabetes: current concepts and future perspectives. Eur Cardiol 2019;14(1):50–9.

[38] Joseph SB, McKilligin E, Pei L, Watson MA, Collins AR, Laffitte BA, et al. Synthetic LXR ligand inhibits the development of atherosclerosis in mice. Proc Natl Acad Sci USA 2002;99(11):7604–9.

[39] Rosenson RS, Brewer Jr. HB, Barter PJ, Bjorkegren JLM, Chapman MJ, Gaudet D, et al. HDL and atherosclerotic cardiovascular disease: genetic insights into complex biology. Nat Rev Cardiol 2018;15(1):9–19.

[40] Watkins SM, Reifsnyder PR, Pan HJ, German JB, Leiter EH. Lipid metabolome-wide effects of the PPARgamma agonist rosiglitazone. J Lipid Res 2002;43(11):1809–17.

[41] Rull A, Geeraert B, Aragones G, Beltran-Debon R, Rodriguez-Gallego E, Garcia-Heredia A, et al. Rosiglitazone and fenofibrate exacerbate liver steatosis in a mouse model of obesity and hyperlipidemia. A transcriptomic and metabolomic study. J Proteome Res 2014;13(3):1731–43.

[42] Adam J, Brandmaier S, Leonhardt J, Scheerer MF, Mohney RP, Xu T, et al. Metformin effect on nontargeted metabolite profiles in patients with type 2 diabetes and in multiple murine tissues. Diabetes 2016;65(12):3776–85.

[43] Jonsson TJ, Schafer HL, Herling AW, Bronstrup M. A metabolome-wide characterization of the diabetic phenotype in ZDF rats and its reversal by pioglitazone. PLoS ONE 2018;13(11):e0207210.

[44] Li YY, Stewart DA, Ye XM, Yin LH, Pathmasiri WW, McRitchie SL, et al. A metabolomics approach to investigate kukoamine B-A potent natural product with anti-diabetic properties. Front Pharmacol 2018;9:1575.

[45] Tomasova J, Buganova M, Pelantova H, Holubova M, Sediva B, Zelezna B, et al. Metabolomics based on MS in mice with diet-induced obesity and Type 2 diabetes mellitus: the effect of vildagliptin, metformin, and their combination. Appl Biochem Biotechnol 2019;188(1):165–84.

[46] Ryan PM, Patterson E, Carafa I, Mandal R, Wishart DS, Dinan TG, et al. Metformin and dipeptidyl peptidase-4 inhibitor differentially modulate the intestinal microbiota and plasma metabolome of metabolically dysfunctional mice. Can J Diabetes 2020;44(2):146–55 e2.

[47] Miao B, Zondlo S, Gibbs S, Cromley D, Hosagrahara VP, Kirchgessner TG, et al. Raising HDL cholesterol without inducing hepatic steatosis and hypertriglyceridemia by a selective LXR modulator. J Lipid Res 2004;45(8):1410–7.

[48] van der Hoorn J, Linden D, Lindahl U, Bekkers M, Voskuilen M, Nilsson R, et al. Low dose of the liver X receptor agonist, AZ876, reduces atherosclerosis in

APOE*3Leiden mice without affecting liver or plasma triglyceride levels. Br J Pharmacol 2011;162(7):1553–63.

[49] Phelan CA, Weaver JM, Steger DJ, Joshi S, Maslany JT, Collins JL, et al. Selective partial agonism of liver X receptor alpha is related to differential corepressor recruitment. Mol Endocrinol 2008;22(10):2241–9.

[50] El-Gendy BEM, Goher SS, Hegazy LS, Arief MMH, Burris TP. Recent advances in the medicinal chemistry of liver X receptors. J Med Chem 2018.

[51] Wagner BL, Valledor AF, Shao G, Daige CL, Bischoff ED, Petrowski M, et al. Promoter-specific roles for liver X receptor/corepressor complexes in the regulation of ABCA1 and SREBP1 gene expression. Mol Cell Biol 2003;23(16):5780–9.

[52] Fan J, Zhao RQ, Parro C, Zhao W, Chou HY, Robert J, et al. Small molecule inducers of ABCA1 and apoE that act through indirect activation of the LXR pathway. J Lipid Res 2018;59(5):830–42.

[53] Seneviratne U, Huang Z, Am Ende CW, Butler TW, Cleary L, Dresselhaus E, et al. Photoaffinity labeling and quantitative chemical proteomics identify LXRbeta as the functional target of enhancers of astrocytic apoE. Cell Chem Biol 2020.

[54] Li N, Wang X, Xu Y, Lin Y, Zhu N, Liu P, et al. Identification of a novel liver x receptor agonist that regulates the expression of key cholesterol homeostasis genes with distinct pharmacological characteristics. Mol Pharmacol 2017;91(4):264–76.

[55] Nomura S, Endo-Umeda K, Makishima M, Hashimoto Y, Ishikawa M. Development of tetrachlorophthalimides as liver X receptor beta (LXRbeta)-selective agonists. ChemMedChem 2016;11(20):2347–60.

[56] Archer A, Stolarczyk E, Doria ML, Helguero L, Domingues R, Howard JK, et al. LXR activation by GW3965 alters fat tissue distribution and adipose tissue inflammation in ob/ob female mice. J Lipid Res 2013;54(5):1300–11.

[57] Thomas J, Bramlett KS, Montrose C, Foxworthy P, Eacho PI, McCann D, et al. A chemical switch regulates fibrate specificity for peroxisome proliferator-activated receptor alpha (PPARalpha) versus liver X receptor. J Biol Chem 2003;278(4):2403–10.

[58] Yao-Borengasser A, Rassouli N, Varma V, Bodles AM, Rasouli N, Unal R, et al. Stearoyl-coenzyme A desaturase 1 gene expression increases after pioglitazone treatment and is associated with peroxisomal proliferator-activated receptor-gamma responsiveness. J Clin Endocrinol Metab 2008;93(11):4431–9.

[59] Hebbachi AM, Knight BL, Wiggins D, Patel DD, Gibbons GF. Peroxisome proliferator-activated receptor alpha deficiency abolishes the response of lipogenic gene expression to re-feeding: restoration of the normal response by activation of liver X receptor alpha. J Biol Chem 2008;283(8):4866–76.

[60] Yamauchi T, Waki H, Kamon J, Murakami K, Motojima K, Komeda K, et al. Inhibition of RXR and PPARgamma ameliorates diet-induced obesity and type 2 diabetes. J Clin Invest 2001;108(7):1001–13.

[61] Kalaany NY, Gauthier KC, Zavacki AM, Mammen PP, Kitazume T, Peterson JA, et al. LXRs regulate the balance between fat storage and oxidation. Cell Metab 2005;1(4):231–44.

[62] Guerre-Millo M, Rouault C, Poulain P, Andre J, Poitout V, Peters JM, et al. PPAR-alpha-null mice are protected from high-fat diet-induced insulin resistance. Diabetes 2001;50(12):2809–14.

[63] Hashidate-Yoshida T, Harayama T, Hishikawa D, Morimoto R, Hamano F, Tokuoka SM, et al. Fatty acid remodeling by LPCAT3 enriches arachidonate in phospholipid membranes and regulates triglyceride transport. Elife 2015;4.

[64] Singh AB, Liu J. Identification of hepatic lysophosphatidylcholine acyltransferase 3 as a novel target gene regulated by peroxisome proliferator-activated receptor delta. J Biol Chem 2017;292(3):884–97.

[65] Rong X, Wang B, Palladino EN, de Aguiar Vallim TQ, Ford DA, Tontonoz P. ER phospholipid composition modulates lipogenesis during feeding and in obesity. J Clin Invest 2017;127(10):3640–51.

[66] Honzumi S, Shima A, Hiroshima A, Koieyama T, Ubukata N, Terasaka N. LXRalpha regulates human CETP expression in vitro and in transgenic mice. Atherosclerosis 2010;212(1):139–45.

[67] Hong C, Marshall SM, McDaniel AL, Graham M, Layne JD, Cai L, et al. The LXR-Idol axis differentially regulates plasma LDL levels in primates and mice. Cell Metab 2014;20(5):910–8.